Highly Efficient Nonlinear Torque Control of Induction Motor Drives Considering Magnetic Saturation and Iron Losses

Mohammad Ali Salahmanesh, Hossein Abootorabi Zarchi, Salman Abdi, *Senior Member, IEEE*, Hamidreza Mosaddegh-Hesar, and Xiaodong Liang, *Senior Member, IEEE*

Abstract— In this paper, an input-output feedback linearization (IOFL)-based direct torque control (DTC) is proposed for induction motor (IM) drives using the maximum torque per Ampere (MTPA) strategy and full nonlinear IM model. In contrast to conventional IOFL technique, the stability of the proposed IOFL is proven by Lyapunov theory. The proposed method not only provides an appropriate tracking of electromagnetic torque, but also leads to an optimal relation between direct (d)quadrature (q) axis stator currents. Since both MTPA strategy and IOFL control depend on the IM model, more accurate dynamic modelling including effects of magnetic saturation and iron losses is essential. In this regard, a fifth-order IM model developed based on a full nonlinear model is used in the controller design by considering variations of magnetizing inductance and iron loss resistance in terms of the magnetic current and rotor speed, respectively. The proposed control scheme is validated by experimental results showing a significant reduction in the stator current for a light load compared to the conventional model, in which saturation and iron losses are neglected.

Index Terms—Input-output feedback linearization (IOFL), induction motor, iron loss resistance, maximum torque per ampere (MTPA), magnetic saturation effect.

Nomenclature

Voltage, flux, current vectors			
Electromagnetic torque			
Resistance			
Stator and rotor leakage inductances			
Magnetizing (static), and dynamic inductances			
D-axis magnetizing inductance			
Q-axis magnetizing inductance			
Cross saturation inductance between orthogonal D-Q axes of stator winding.			
The number of pole pairs			
Angular speed of arbitrary reference frame			
Rotor angular speed			
Angle of magnetizing current with respect to D-axis of arbitrary reference frame.			
Stator, rotor			
Magnetizing, core			
Two-axis arbitrary reference frame			
Direct and quadrature axes of the rotor flux reference frame			
Two-axis stationary reference frame			

I. INTRODUCTION

YNAMIC behavior analysis of induction motors (IMs) can be improved by accurately modelling the saturation effect and iron losses. However, the conventional model of IMs neglects the iron losses and variation in magnetization. Neglecting iron losses may cause errors when calculating the slip, rotor flux and electromagnetic torque in an IM model [1-3]. In various applications, such as field weakening and traction, magnetic saturation phenomena can significantly affect behaviors of the IM drive [4, 5]. Nevertheless, the magnetizing saturation effect is rarely considered in control designs due to its mathematical complexity [6]. The combined impact of iron loss and saturation effect on vector-controlled IM operation is investigated in [7]. Both these effects are covered by evaluating of detuning in transient and steady-state operation and modifying rotor flux estimators that compensate detuning factors. It is shown that the modified estimators, which compensate both phenomena, require two non-linear functions, the magnetizing curve of machine and iron loss variation in terms of frequency.

In electrical machines modelling, two approaches are generally used to consider the magnetic saturation effect. In the first approach, known as the "simplified model", a variable inductance, which is a non-linear function of the magnetizing current, is used rather than a constant magnetizing inductance [8-10]. In the second approach, a full non-linear model is used, in which voltage equations are obtained differing from an unsaturated model due to time variations of the magnetizing inductance and new terms representing the cross-saturation effect [11]. This full non-linear IM model shows superior performance compared to the simplified model due to faster response and higher accuracy [12, 13].

In [14, 15], a general procedure of saturation modelling is studied for two-axis frame models of IMs by selecting different state variables. These models can be categorized into three separate groups based on the needs to fulfill the time derivative of the magnetizing inductance, its inverse, or none of them. Cross-saturation terms appear in the first two groups. In the first group, all models that require the time derivative of the magnetizing inductance show poor accuracy if the cross-saturation terms are omitted. In the second group, neglecting

the cross-saturation has little influence on the models that require a time derivative of the inverse of the magnetizing inductance. Therefore, the cross-saturation must be considered in the first group. Ref. [16] proposes a method for general modelling of the saturation effect based on a full non-linear model and iron losses in the two-axis electric machine model. By imposing constraints on the general model, synchronous, induction, and DC machine equations are obtained. Thus, to model the saturation effect, the cross-saturation terms are included in the IM model according to the first group, in this paper.

To deal with highly nonlinear systems, nonlinear control methods, such as IOFL, are recommended by the control theory. The IOFL technique transforms a nonlinear system into a system with linear dynamics by applying a feedback control and changing coordinates [17]. Applying IOFL for IMs drive system has several advantages, such as the control feasibility in a wider operation range, better stability of the drive system, and being appropriate for incorporating highly nonlinear parameters, including hysteresis and saturation effects [18]. In the literature, research has been conducted by incorporating saturation effect in the IM model and its control design. In [19], the IOFL control for IMs is proposed that takes into account the magnetic saturation effect of the iron core in the rotor flux reference frame. Using non-linear function interpolating, the magnetizing inductance is derived in terms of the rotor magnetizing current, resulting in the increase in the nonlinearity of IM equations. This reference shows that the proposed IOFL is developed through a more accurate modeling procedure for saturation effect. In [6], an IOFL-based tracking control of IMs is improved by including magnetic saturation. Variable states are chosen as the mixed "rotor flux linkage-stator currents" in the stationary reference frame. This method shows superior performance with smaller rotor position and speed errors than the unsaturated control method. Considering saturation in the rotor flux linkage observer design also enhances operation of the controlled IM.

By considering iron losses, the current flowing through the iron loss resistance must be defined as an additional state variable, which makes non-linear controller design more complex. In [20], a non-linear technique considering iron losses for IM drives is developed, where the iron loss resistance (assumed as a constant) is in parallel with the rotor resistance in the rotor magnetizing current reference frame. Therefore, the iron loss is modelled without adding new state variables. In [21], an adaptive nonlinear DTC of IM drives based on integrator backstepping is presented. The iron loss resistance, dependent on the synchronous speed, is determined by no-load tests.

In electric machine control, the maximum torque per Ampere (MTPA) control strategy aims to deliver the electromagnetic torque with the lowest current magnitude, through which copper losses are minimized and the efficiency can be improved [22-24]. Incorporating iron loss and saturation effects into the MTPA control is often ignored in the literature, although it can improve the control accuracy. In [25], a simple MTPA algorithm is combined with the predictive control to determine

the optimal stator current angle; this method is valid in a wide range of operating points, but the optimization is not performed due to speed and electromagnetic torque variations. In [26], a MTPA strategy based on the scalar control is used to minimize the stator current of IMs. In [27], two MTPA control strategies are proposed to improve the efficiency of IM drives in electric vehicle (EV) applications. In [28], two MTPA methods are presented to determine the optimal stator current value for IMs and interior permanent magnet synchronous motors (IPMSMs); the first method is developed based on a motor model considering saturation, and the second method is a new searchbased online optimization scheme. In [29], a novel MTPA fieldoriented controller is proposed for IM drives by maximizing the electromagnetic torque per ampere ratio when the load torque is slow varying or constant, which guarantees the speed (electromagnetic torque) tracking of reference trajectories. Wasynczuk et al. in [30] propose a MTPA control strategy using the slip speed control, implemented through indirect field-oriented control (FOC) in the rotor flux reference frame; to implement this strategy, the slip speed should be equal to the rotor time constant, and the stator currents on the direct- and quadrature-axis are equalized, serving as the realization criterion for MTPA (iron losses in the IM are not considered). In [31], the optimal flux for a desired load torque is determined by a look-up table for the MTPA control without considering iron losses. In [32], a predictive MTPA strategy is proposed based on direct torque and flux control without considering iron losses, and this strategy is only effective for high-torque and high-speed applications. To date, the iron loss and saturation effects have not been considered simultaneously in the literature for the MTPA control.

To fill the research gap, an improved model that simultaneously considers the effects of saturation and iron losses is presented. Its benefits include: 1) Incorporating the variation of the iron loss resistance with the supply voltage frequency, 2) Modifying voltage equations based on the saturation effect and considering magnetizing cross-coupling terms between the two axes, 3) Eliminating the need to define a new state variable for IOFL design due to the iron loss branch, and 4) Strong prediction of the torque transient. Adopting the improved model, the main contributions of this paper include:

- To improve the performance of IM drives, an IOFL-based nonlinear torque control is proposed, and the stability of the proposed controller is proven by Lyapunov theory. The IM's fifth-order model used in the controller design is developed by adopting a full nonlinear model based on both iron losses and magnetic saturation effects.
- 2) An accurate MTPA-based control strategy is developed for IM drives, in which iron losses and the saturation effect are considered simultaneously in the MTPA design. The optimal stator current angle obtained using the gradient method is deviated to a value bigger than π/4 rad due to incorporating iron losses and magnetic saturation. The proposed nonlinear controller meets the MTPA strategy in the stationary reference frame when the stator current magnitude tracks its reference value obtained by the MTPA

strategy.

The paper is organized as follows: in Section II, the dynamic model of IMs is introduced by taking saturation effect and iron losses into account; in Section III, the optimal relation is determined between two-axis stator currents according to the MTPA strategy, and the saturation phenomenon and iron losses are considered as two possible sources of performance degradation in the MTPA strategy; in Section IV, the Lyapunov-based IOFL is obtained for the IM drive in the stationary reference frame; in Section V, experimental results are presented to validate the proposed method; and concluding remarks are summarized in Section VI.

II. TWO AXIS MODEL OF IMS INCLUDING IRON LOSSES AND SATURATION EFFECT

A. Step 1- Considering magnetic saturation effect

In this section, the saturation effect is modelled through voltage equations. The space vector equations of an ideal IM model, in which iron losses and the effect of magnetic saturation are ignored, can be expressed in an arbitrary reference frame as follows [12]:

$$\vec{V}_s = R_s \vec{I}_s + L_{ls} \frac{d\vec{I}_s}{dt} + \frac{d\vec{\lambda}_m}{dt} + j\omega \vec{\lambda}_s$$
 (1)

$$\vec{V}_r = R_r \vec{I}_r + L_{lr} \frac{d\vec{I}_r}{dt} + \frac{d\vec{\lambda}_m}{dt} + j(\omega - \omega_r) \vec{\lambda}_r$$
 (2)

where $\vec{\lambda}_m = L_m \vec{I}_m$ is the magnetizing flux vector. This model is often used in the literature, ignoring the magnetic saturation, and hence using a constant magnetizing inductance. By taking the magnetic saturation into account, parameters, such as magnetizing inductance, and stator and rotor inductances, are varied with operating conditions. Voltage equations in the presence of saturation can be derived by replacing time-varying magnetizing inductance into linear magnetic voltage equations. To consider variations of the magnetizing inductance, the derivative of D- and Q-axis components of the magnetizing flux linkage in the arbitrary reference frame can be written by

$$\frac{d\lambda_{mD}}{dt} = L_m \frac{dI_{mD}}{dt} + I_{mD} \frac{dL_m}{dt}
\frac{d\lambda_{mQ}}{dt} = L_m \frac{dI_{mQ}}{dt} + I_{mQ} \frac{dL_m}{dt}$$
(3)

$$\frac{d\lambda_{mQ}}{dt} = L_m \frac{dI_{mQ}}{dt} + I_{mQ} \frac{dL_m}{dt} \tag{4}$$

The first-time derivative of the magnetizing inductance due to saturation condition can be computed as follows [11], [12]:

$$\frac{dL_m}{dt} = \left(\frac{L - L_m}{|\vec{I}_m|}\right) \frac{d|\vec{I}_m|}{dt} \tag{5}$$

The static and dynamic inductances in (5), are determined by

$$L_m = \frac{|\vec{\lambda}_m|}{|\vec{l}_m|} \qquad L = \frac{d|\vec{\lambda}_m|}{d|\vec{l}_m|} \tag{6}$$

The dynamic inductance introduced under this condition differentiates the full nonlinear model from the simplified model. In the full nonlinear model, these inductances have different values, whereas in the simplified model, they are equal, causing (5) equal to zero. In (5), the time derivative of the magnetizing current's space phasor magnitude is determined by

$$\frac{d|\vec{l}_m|}{dt} = \frac{dI_{mD}}{dt}\cos\mu + \frac{dI_{mQ}}{dt}\sin\mu \tag{7}$$

Since the expression of $d|\vec{l}_m|/dt$ appeared in (5) depends on both D and Q-axis components of the magnetizing current, the cross-coupling term is created in (3) and (4) by dL_m/dt . Therefore, the first-time derivative of the magnetizing flux can be restated by substituting (5) into (3) and (4) as follows:

$$\frac{d\lambda_{mD}}{dt} = L_{mD} \frac{dI_{mD}}{dt} + L_{DQ} \frac{dI_{mQ}}{dt} \tag{8}$$

$$\frac{d\lambda_{mD}}{dt} = L_{mD} \frac{dI_{mD}}{dt} + L_{DQ} \frac{dI_{mQ}}{dt}$$

$$\frac{d\lambda_{mQ}}{dt} = L_{mQ} \frac{dI_{mQ}}{dt} + L_{DQ} \frac{dI_{mD}}{dt}$$
(8)

Referring to (6), and after some manipulations, L_{mD} , L_{mQ} and L_{DO} are obtained as follows:

$$L_{mD} = L\cos^2\mu + L_m\sin^2\mu \tag{10}$$

$$L_{mD} = L \cos^2 \mu + L_m \sin^2 \mu$$
 (10)

$$L_{mQ} = L \sin^2 \mu + L_m \cos^2 \mu$$
 (11)

$$L_{DO} = (L - L_m) \sin\mu \cos\mu \tag{12}$$

The above equations can be used for both stationary and rotating reference frames (for instance, the rotor flux frame), only by modifying the angle of the magnetizing current's space phasor. According to Fig. 1, if the angle μ is replaced by μ_r , these equations can be used for the stationary reference frame. According to (10)-(12), the magnetizing inductance along D and O axes are different. Moreover, there is a magnetic coupling between the orthogonal axes, which is modelled by a crosscoupling inductance. These inductances are incorporated into the voltage equations leading to a modified IM model. Under linear conditions, static and dynamic inductances are equal, $L_{mD} = L_{mQ} = L_m$ and $L_{DQ} = 0$. To obtain static and dynamic inductances, the characteristic curve of the machine must be determined. In this way, the saturation in the main flux path, and static and dynamic inductances can be defined as a function of the magnetizing current, as shown in Appendix. Due to the magnetizing curve, the static inductance is equal to the slop of a straight line that connects the origin to each operating point. Similarly, the tangential slop of the magnetizing curve at a given operating point is defined as the dynamic inductance. As shown in this section, not only all inductances are modified in the saturated model, but also D- and Q- axis equivalent circuits are coupled together due to the cross-saturation effect. Although, the electromagnetic torque expression is the same in both saturation and linear models since no additional terms are introduced for the saturation phenomenon, variations in the inductance values as well as stator and magnetizing currents indirectly affects the electromagnetic torque.

B. Step 2- The saturated IM model with including iron losses

Ignoring iron losses can cause errors when calculating the slip, rotor flux and electromagnetic torque in an IM model. The iron loss resistance is in parallel with the magnetizing inductance in the stationary reference frame. A more accurate IM model is obtained considering the iron loss resistance, which varies with the synchronous speed. The equivalent iron loss resistance, R_c , of the 2.2 kW IM can be experimentally

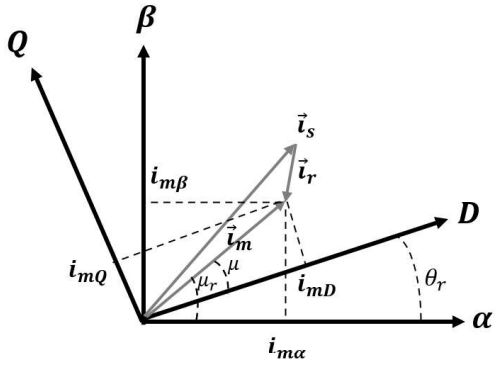


Fig. 1. Space phasor diagram of the magnetizing current. identified by measuring the input power at the no-load test using the approach established in IEEE standard 112 [33]. The energy balance of an induction motor under no-load condition can be expressed by

$$P_{no-load} = P_{iron} + P_{cu,s} + P_{mech} \tag{13}$$

where P_{iron} , $P_{cu.s}$ and P_{mech} are the iron loss, the stator copper loss, and friction and windage losses, respectively. Based on [33], the iron loss, P_{iron} , a difference between the input/no-load power $P_{no-load}$ and other losses, can be computed by (13). The no-load power is calculated at various frequencies. To determine the friction and windage loss, the no-load power is recorded, and the stator's RI^2 loss is then subtracted from the no-load power at each of the test voltage points. The resulting power curve is plotted versus the square of the excitation voltage, extending the curve to zero voltage. The approximate friction and windage losses are obtained by finding the intersection point of this curve and the power axis. By determining the stator copper losses under various loading conditions, the iron loss at each test voltage is obtained by subtracting the value of friction and windage losses from the no-load power minus the stator's RI^2 loss. R_c is more sensitive to the variation of the operating frequency than to the variation of the flux level [34, 35]. Fig. 2 shows variations of the iron loss resistance in terms of the supply frequency, and can be used in determining the iron loss at any desired rotor speed. In the stationary reference frame, Kirchhoff's voltage law (KVL) can be used in the equivalent circuit of the saturated IM to obtain iron losses as follows:

$$R_c \vec{I}_c^s = \frac{d\vec{\lambda}_m^s}{dt} = \frac{d(L_m \vec{I}_m^s)}{dt}$$
 (14)

where the superscript "s" indicates the stationary reference frame. According to the conversion between frames as \vec{x}_2 = $\vec{x}_1 e^{-j\theta}$, in which \vec{x}_2 , \vec{x}_1 are space vectors in the new and old frames, respectively, and θ is equal to angular replacement of the new frame with respect to the old frame, Eq. (14) can be rewritten in the arbitrary reference frame as follows:

$$R_c \vec{I}_c^a e^{j\theta} = \frac{d(L_m \vec{I}_m^a e^{j\theta})}{dt} = L_m e^{j\theta} \frac{d\vec{I}_m^a}{dt} + j\omega e^{j\theta} L_m \vec{I}_m^a + \vec{I}_m^a e^{j\theta} \frac{dL_m}{dt}$$

$$(15)$$

By substituting (5) into (15), the voltage vector across the iron loss branch can be obtained:

$$R_c \vec{l}_c = L_m \frac{d\vec{l}_m}{dt} + j\omega L_m \vec{l}_m + \vec{l}_m \left(\frac{L - L_m}{|\vec{l}_m|}\right) \frac{d|\vec{l}_m|}{dt}$$
 (16)

Considering (7), (16) can be expressed in two axes arbitrary reference frame as follows:

$$\begin{split} R_c(I_{cD}+jI_{cQ}) &= L_m \frac{d(I_{mD}+jI_{mQ})}{dt} + j\omega L_m(I_{mD}+jI_{mQ}) + \\ (I_{mD}+jI_{mQ}) \left(\frac{L-L_m}{|\vec{I}_m|}\right) \left[\frac{dI_{mD}}{dt} cos\mu + \frac{dI_{mQ}}{dt} sin\mu\right] \end{split} \tag{17}$$

The D-axis component of (16) can be computed by

$$\begin{split} R_c I_{cD} &= L_m \frac{dI_{mD}}{dt} - \omega L_m I_{mQ} \\ &+ \left(I_{mD} \frac{L - L_m}{|\vec{I}_m|} \right) \left(\frac{dI_{mD}}{dt} \cos \mu + \frac{dI_{mQ}}{dt} \sin \mu \right) \end{split} \tag{18}$$

By taking $I_{mD} = |\vec{I}_m| \cos \mu$ and $I_{mQ} = |\vec{I}_m| \sin \mu$ into account and after some straightforward computations, the above equation can be rewritten for the D-axis as follows:

$$\begin{split} R_c I_{cD} &= L_m \frac{dI_{mD}}{dt} - \omega L_m I_{mQ} + (L - L_m) \left[\frac{dI_{mD}}{dt} cos^2 \mu + \frac{dI_{mQ}}{dt} cos\mu. sin\mu \right] = L_m \frac{dI_{mQ}}{dt} - \omega L_m I_{mQ} + Lcos^2 \mu \frac{dI_{mD}}{dt} + \\ Lcos\mu. sin\mu \frac{dI_{mQ}}{dt} - L_m cos^2 \mu \frac{dI_{mD}}{dt} - L_m cos\mu. sin\mu \frac{dI_{mQ}}{dt} \end{split} \tag{19}$$

Finally, by considering the defined inductance values in (10-12) and substituting them into (19), Eq. (18) can be stated into the two-axis rotating reference frame as follows:

$$R_{c}I_{cD} = L_{mD}\frac{dI_{mD}}{dt} + L_{DQ}\frac{dI_{mQ}}{dt} - \omega L_{m}I_{mQ}$$

$$R_{c}I_{cQ} = L_{mQ}\frac{dI_{mQ}}{dt} + L_{DQ}\frac{dI_{mD}}{dt} + \omega L_{m}I_{mD}$$
(20)

$$R_c I_{cQ} = L_{mQ} \frac{a I_{mQ}}{dt} + L_{DQ} \frac{a I_{mD}}{dt} + \omega L_m I_{mD}$$
 (21)

The speed voltage terms along D-Q axes of the arbitrary reference frame can appear either in the iron loss branch or the magnetizing branch. When placed in the magnetizing branch, the series speed voltages in both the stator and rotor branches must be adjusted. In contrast, placing these terms in the iron loss branch preserves the apparent form of the equivalent circuit. Therefore, in this study, speed voltages along the D-Q axes of the arbitrary reference frame are considered in series with the iron loss resistance. Therefore, based on Steps 1 and 2, a two-axis frame model of an IM in the arbitrary reference frame and with the effects of saturation and iron losses into account, can be derived as shown in Fig. 3. The dynamic performance of the full nonlinear model of Fig. 3 is studied during free acceleration with the full load torque.

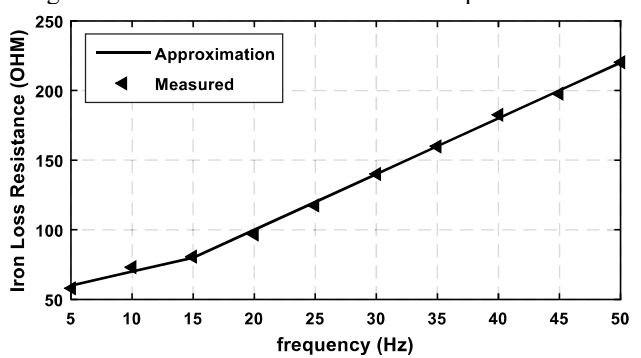


Fig. 2. The measured iron loss resistance at different frequencies for the 2.2 kW

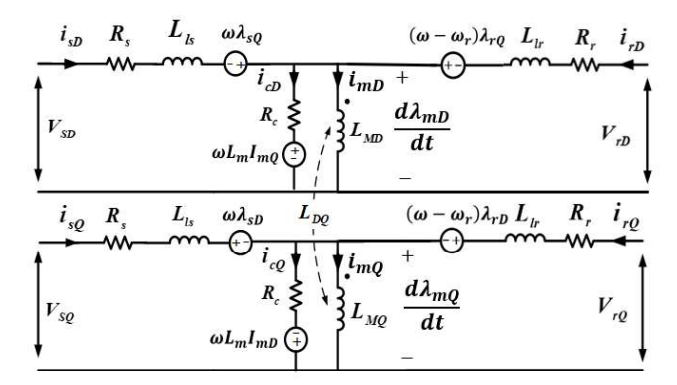


Fig. 3. The equivalent circuit of an IM in the two-axis arbitrary reference frame including iron losses and the saturation effect.

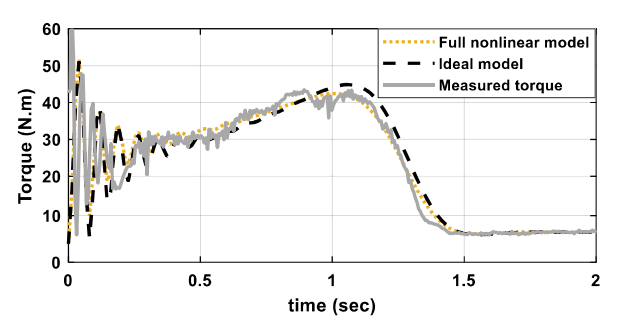


Fig. 4. Comparison of the electromagnetic torque behavior in ideal and full nonlinear models (free acceleration).

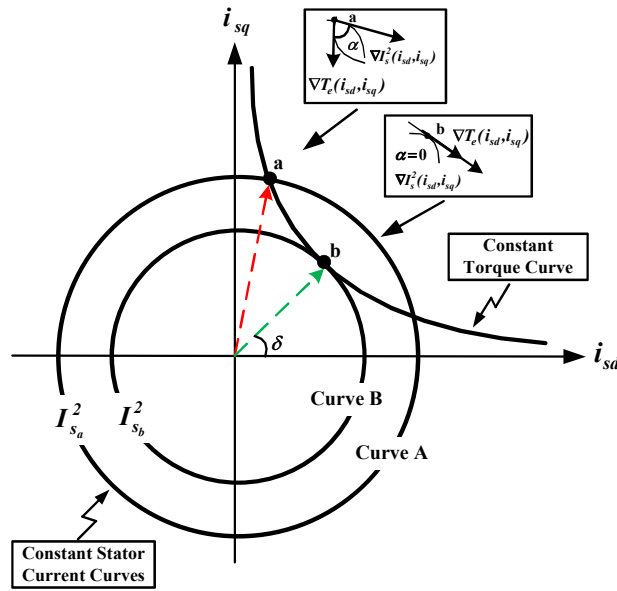


Fig. 5. Constant electromagnetic torque curve and stator current curves.

Electromagnetic torque curves for the ideal, full nonlinear models and measured value are shown in Fig. 4. As expected, the torque amplitude of the full nonlinear model is smaller than that of the ideal model during transient due to considering the saturation effect and iron losses in the IM model.

III. THE MTPA STRATEGY FOR IMS

The main goal of MTPA strategies is to provide the required electromagnetic torque with the lowest magnitude of the stator current. In this paper, the MTPA strategy is introduced based on Lagrange's theorem. To implement the proposed MTPA strategy, the electromagnetic torque should be expressed in terms of two-axis components of the stator current in the rotor flux reference frame as [36]:

$$T_e = \frac{3P}{2} \frac{L_m}{L_r} \left(\frac{R_c}{\beta \omega} \right) \left(i_{sd} \ i_{sq} - \frac{i_{sd}^2}{\beta} \right) \tag{22}$$

where $\beta = R_c/\omega L_m$.

The electromagnetic torque expression can be drawn on the $i_{sd}-i_{sq}$ plane. The square stator current curve is circular in this plane. With a constant electromagnetic torque restriction, curve "A" is taken to represent the corresponding constant stator current curve if the operating point is fixed at point "a" in Fig. 5. When an operating point is changed to "b," the "B" curve becomes the new constant stator current curve. When the square stator current curve and the constant electromagnetic torque curve are tangent at a point, according to Lagrange's theorem, the stator current is at its minimum value. This simply indicates that the MTPA is realized when their gradient vectors are parallel at the tangent point. So that,

$$\|\nabla T_e(i_{sd}, i_{sq})\| \|\nabla I_s^2(i_{sd}, i_{sq})\| \sin \alpha = 0$$
(23)

The general criterion for realizing the MTPA strategy can be expressed by

$$y_1 = \|\nabla T_e(i_{sd}, i_{sq})\| \|\nabla I_s^2(i_{sd}, i_{sq})\| \sin \alpha$$
 (24)

As clear, the control strategy is realized when y_1 remains zero. The cross product of the gradient vectors is calculated by

$$\nabla T_{e}(i_{sd}, i_{sq}) \times \nabla I_{s}^{2}(i_{sd}, i_{sq}) = det \begin{bmatrix} i & j & k \\ \frac{\partial T_{e}}{\partial i_{sd}} & \frac{\partial T_{e}}{\partial i_{sq}} & 0 \\ \frac{\partial I_{s}^{2}}{\partial i_{sd}} & \frac{\partial I_{s}^{2}}{\partial i_{sq}} & 0 \end{bmatrix}$$
(25)

Therefore, the MTPA realization criterion is expressed by

$$\begin{aligned} y_1 &= \frac{\partial T_e}{\partial i_{sd}} \times \frac{\partial I_s^2}{\partial i_{sq}} - \frac{\partial T_e}{\partial i_{sq}} \times \frac{\partial I_s^2}{\partial i_{sd}} = 0 \Rightarrow y_1 \\ &= i_{sq}^2 - \frac{2}{\beta} i_{sq} i_{sd} - i_{sd}^2 = 0 \end{aligned} \tag{26}$$

Under the ideal condition, the optimal current angle is constant $(\delta = \pm \pi/4 \, rad)$. Under non-ideal condition, to overcome the effect of iron losses and magnetic saturation, the stator current angle will be bigger than $\pi/4 \, rad$, depending on the value of β . From (26), we have

$$i_{sq} = \pm i_{sd}\xi \Rightarrow \delta = tan^{-1}(\xi)$$
 (27)

where $\xi=\left(\frac{\sqrt{\beta^2+1}+1}{\beta}\right)$ is the MTPA factor. Eq. (27) shows that $i_{sq}-\xi i_{sd}=0$ must always apply to

Eq. (27) shows that $i_{sq} - \xi i_{sd} = 0$ must always apply to realize the MTPA in motoring mode of operation. Hence, it is necessary to determine the value of ξ for any given frequency, as shown in Fig. 6. Fig. 7 shows the deviation of the stator current angle from $\pi/4$ rad at different frequencies due to iron losses and saturation effect. To satisfy the MTPA strategy, Figs. 6 and 7 are used in the proposed control scheme and effects of them are shown in the experimental results.

$$f(x) = \begin{bmatrix} \frac{1}{L_{ls}} \left(-(R_r + (R_s || R_c)) x_1 + R_r x_3 + x_5 L_m x_4 \right) \\ \frac{1}{L_{ls}} \left(-(R_r + (R_s || R_c)) x_2 + R_r x_4 - x_5 L_m x_3 \right) \\ A(L_{M\beta} x_1 - L_{\alpha\beta} x_2 - (BL_{\alpha\beta} + L_{M\beta}) x_3 + (L_{\alpha\beta} - BL_{M\beta}) x_4 \right) \\ A(L_{M\alpha} x_2 - L_{\alpha\beta} x_1 + (L_{\alpha\beta} + BL_{M\alpha}) x_3 + (BL_{\alpha\beta} - L_{M\alpha}) x_4 \right) \\ \frac{1}{p_j} (T_e - T_l) \end{bmatrix}, \quad g_1(x) = \begin{bmatrix} \frac{1}{L_{ls}} \\ 0 \\ 0 \\ 0 \end{bmatrix} \qquad g_2(x) = \begin{bmatrix} \frac{0}{1} \\ \frac{1}{L_{ls}} \\ 0 \\ 0 \\ 0 \end{bmatrix}$$
(29)

IV. NONLINEAR CONTROLLER DESIGN

In this section, the IOFL technique is introduced based on the proposed model by incorporating effects of saturation and iron losses of the machine. The IOFL approach can transform behaviors of a non-linear system, such as IMs to a linear system using a new set of coordinates and feedback control. The IOFL control was mainly applied to IM drives when saturation effects were ignored. However, this study attempts to consider both saturation effect and iron losses as decisive factors for highly accurate operation of this approach. The fifth-order model of IMs with stator currents $(i_{s\alpha}, i_{s\beta})$, magnetizing currents $(i_{m\alpha}, i_{m\beta})$ and the rotor speed as state variables in the stationary reference frame can be expressed by

$$\dot{x} = f(x) + g_1(x)V'_{s\alpha} + g_2(x)V'_{s\beta}$$
(28)

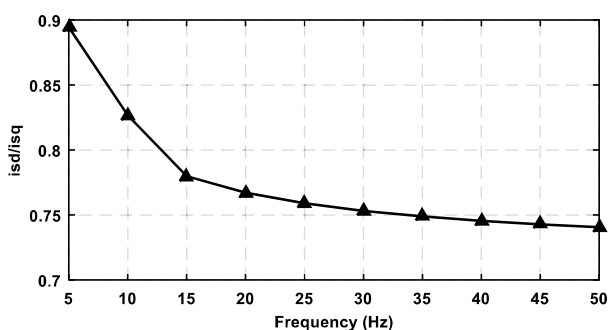


Fig. 6. Variations of i_{sd}/i_{sq} with the operating frequency.

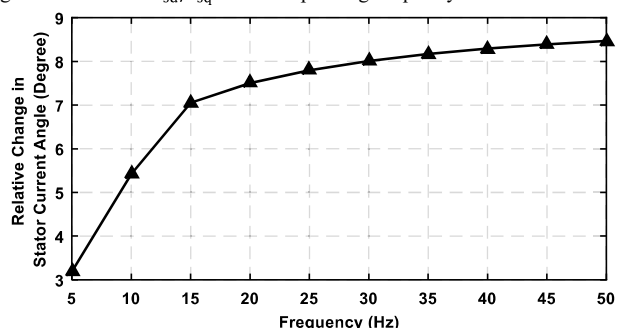


Fig. 7. Relative changes in the stator current angle with frequency.

$$\frac{i_{s\alpha} \quad R_{s} \| R_{c}}{R_{c} + R_{s}} V_{s\alpha} = V'_{s\alpha} \qquad \frac{i_{s\beta} \quad R_{s} \| R_{c}}{R_{c} + R_{s}} V_{s\beta} = V'_{s\beta}$$

Fig. 8. Thevenin equivalent circuit through the iron loss branch.

where $x = [i_{s\alpha}, i_{s\beta}, i_{m\alpha}, i_{m\beta}, \omega_r]$, and $f(x), g_1(x)$ and $g_2(x)$ are non-linear functions of state variables, which are subsequently defined as (29).

To eliminate the additional state variable associated with the iron loss resistance branch, this resistance has been moved closer to the stator resistance, and the Thevenin equivalent circuit is represented in Fig. 8. Thus, $V'_{s\alpha}$ and $V'_{s\beta}$ denote Thevenin voltages through the iron loss branch. Coefficients A and B, in (29) can be expressed by

$$A = \frac{R_r}{\left(L_{M\alpha}L_{M\beta} - L_{\alpha\beta}^2\right)} \qquad B = \frac{x_5 L_m}{R_r} \tag{30}$$

It should be noted that magnetizing currents are chosen as state variables to incorporate the saturation effect in the controller design. Iron losses are also considered so that no new state variable defined, simplifying the design procedure of the controller. To track the torque reference and to realize the MTPA strategy, the following error signals are defined:

$$e_1 = y_1 - y_{1ref} (31)$$

$$e_2 = y_2 - y_{2ref} (32)$$

where y_1 and y_2 indicate square of stator current magnitude and electromagnetic torque, respectively. To realize the MTPA strategy by the proposed controller, the square of stator current magnitude must be forced to its reference value which is calculated based on (27). The error dynamics are introduced by

$$e_1 = |\vec{I}_s|^2 - |\vec{I}_s|_{ref}^2 \tag{33}$$

$$e_2 = T_e - T_{eref} \tag{34}$$

The error dynamics, e_1 and e_2 , can be restated as follows:

$$\begin{bmatrix} \dot{e}_{1} \\ \dot{e}_{2} \end{bmatrix} = \begin{bmatrix} L_{f}e_{1} \\ L_{f}e_{2} \end{bmatrix} + \begin{bmatrix} L_{g1}e_{1} & L_{g2}e_{1} \\ L_{g1}e_{2} & L_{g2}e_{2} \end{bmatrix} \begin{bmatrix} V'_{s\alpha} \\ V'_{s\beta} \end{bmatrix} - \begin{bmatrix} |\dot{I}'_{s}|^{2} \\ \dot{T}_{ref} \end{bmatrix}$$
(35)

where Lie derivative functions of the first tracking error are given by:

$$\begin{split} L_{f}e_{1} &= 2 x_{1} \left(\frac{1}{L_{ls}} \left(-\left(R_{r} + \left(R_{s} \| R_{c} \right) \right) x_{1} + R_{r} x_{3} + L_{m} x_{4} x_{5} \right) \right) \\ &+ 2 x_{2} \left(\frac{1}{L_{ls}} \left(-\left(R_{r} + \left(R_{s} \| R_{c} \right) \right) x_{2} + R_{r} x_{4} - L_{m} x_{3} x_{5} \right) \right) \end{split}$$

$$L_{g1}e_{1} &= \frac{2x_{1}}{L_{ls}} \qquad L_{g2}e_{1} = \frac{2x_{2}}{L_{ls}}$$

$$(36)$$

The electromagnetic torque is obtained in the stationary reference frame by

$$T_e = \frac{3}{2} P L_m(x_3 x_2 - x_4 x_1) \tag{37}$$

Due to (37), the Lie derivative functions of the second tracking error are determined by

$$L_{f}e_{2} = \frac{3}{2}PL_{m}\left(\frac{-x_{4}}{L_{ls}}\left(-\left(R_{r} + \left(R_{s} \| R_{c}\right)\right)x_{1} + R_{r}x_{3} + L_{m}x_{4}x_{5}\right) + \frac{x_{3}}{L_{ls}}\left(-\left(R_{r} + \left(R_{s} \| R_{c}\right)\right)x_{2} + R_{r}x_{4} - L_{m}x_{3}x_{5}\right) + x_{2}A\left(L_{M\beta}x_{1} - L_{\alpha\beta}x_{2} - \left(BL_{\alpha\beta} + L_{M\beta}\right)x_{3} + \left(L_{\alpha\beta} - BL_{M\beta}\right)x_{4}\right) - x_{1}A\left(L_{M\alpha}x_{2} - L_{\alpha\beta}x_{1} + \left(L_{\alpha\beta} + BL_{M\alpha}\right)x_{3} + \left(BL_{\alpha\beta} - L_{M\alpha}\right)x_{4}\right)\right)$$

$$L_{g1}e_{2} = -\frac{3}{2}PL_{m}\frac{x_{4}}{L_{ls}} \qquad L_{g2}e_{2} = \frac{3}{2}PL_{m}\frac{x_{3}}{L_{ls}}$$
(38)

In this study, control inputs are chosen so that the Lyapunov stability criteria can be satisfied by the following Lyapunov function candidate:

$$V = \frac{1}{2}(e_1^2 + e_2^2) \tag{39}$$

The time derivative of this function can be derived by substituting error dynamics (35) as follows:

$$\dot{V} = e_1 \dot{e}_1 + e_2 \dot{e}_2
e_1 \left(L_f e_1 + L_{g1} e_1 V_{s\alpha}' + L_{g2} e_1 V_{s\beta}' - \left| \dot{\vec{I}}_s \right|_{ref}^2 \pm \alpha e_1 \right) +
e_2 \left(L_f e_2 + L_{g1} e_2 V_{s\alpha}' + L_{g2} e_2 V_{s\beta}' - \dot{T}_{eref} \pm \beta e_2 \right)$$
(40)

If the control laws are chosen as:

$$\begin{bmatrix} V_{s\alpha} \\ V_{s\beta} \end{bmatrix} = \begin{bmatrix} L_{g1}e_1 & L_{g2}e_1 \\ L_{g1}e_2 & L_{g2}e_2 \end{bmatrix}^{-1} \frac{R_s + R_c}{R_c} \begin{bmatrix} -L_f e_1 - \alpha e_1 + \left| \dot{\vec{T}}_s \right|^2_{ref} \\ -L_f e_2 - \beta e_2 + \dot{T}_{eref} \end{bmatrix}$$
(41)

The time derivative of Lyapunov function becomes:

$$\dot{V} = -\alpha e_1^2 - \beta e_2^2 \tag{42}$$

where α and β must be positive constants to ensure that the derivative of the Lyapunov function is negative definite. The larger these positive constants are chosen, the faster the convergence rate becomes. However, large values for these coefficients increase the control effort, causing higher harmonic distortions in the inverter currents, and degrading the quality of the IM's supply. On the other hand, if these coefficients are too small, the convergence rate decreases, resulting in a slower system dynamic response.

V. EXPERIMENTAL RESULTS AND DISCUSSIONS

The experimental setup shown in Fig. 9 consists of a 2.2 kW IM coupled to a DC generator, and driven by the control drive system hardware based on the Texas Instruments TMS320F28379D DSP platform. Table I shows specifications of the 2.2 kW prototype IM.

TABLE I 2.2 KW IM PARAMETERS

Parameter	Value	Parameter	Value
Rated torque (N.m)	8	$R'_r(\Omega)$	0.6
Rated voltage (V)	220 (L-L)	$L_{ls} = L'_{lr}$ (H)	0.00365
Rated current (A)	8	$L_m(H)$	0.2133
$R_s(\Omega)$	0.76	J (Kg.m ²)	0.038

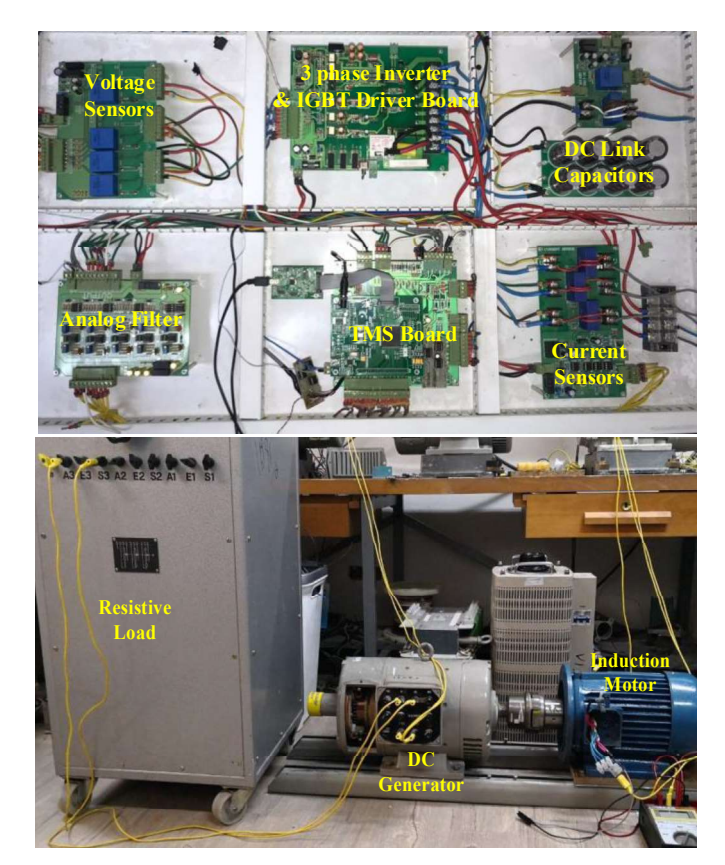


Fig. 9. 2.2 kW induction motor experimental setup.

The block diagram of the drive system is shown in Fig. 10. In the IOFL controller, the stator current magnitude squared serves as one of the control outputs, and its corresponding reference value is determined by the MTPA. In the controller block, to implement the control laws, electrical parameters, such as stator currents and magnetizing currents, along with the variable magnetizing inductance and variable iron loss resistance, are utilized as inputs. To calculate the magnetizing current, the relationship between the stator flux and stator current, along with (44), is used to solve a nonlinear equation and determine the magnetizing current and the magnetizing inductance.

Fig. 11 illustrates IOFL-based controller operation so that satisfies both control objectives of the electromagnetic torque and the MTPA strategy criterion, as shown in Figs. 11(a) and 11(b). This criterion always fluctuates around its reference value, indicating the strategy is realized. Fig. 11(c) shows that the rotor speed increases and decreases linearly, which indicates non-linear controller that the proposed forces electromagnetic torque to track the reference value. As 11(d), the ratio observed Fig. of component to d-axis component of the stator current in the rotor flux reference frame is equal to ξ based on (27). This coefficient introduced earlier in Section III is a function of the iron loss resistance magnetic saturation.

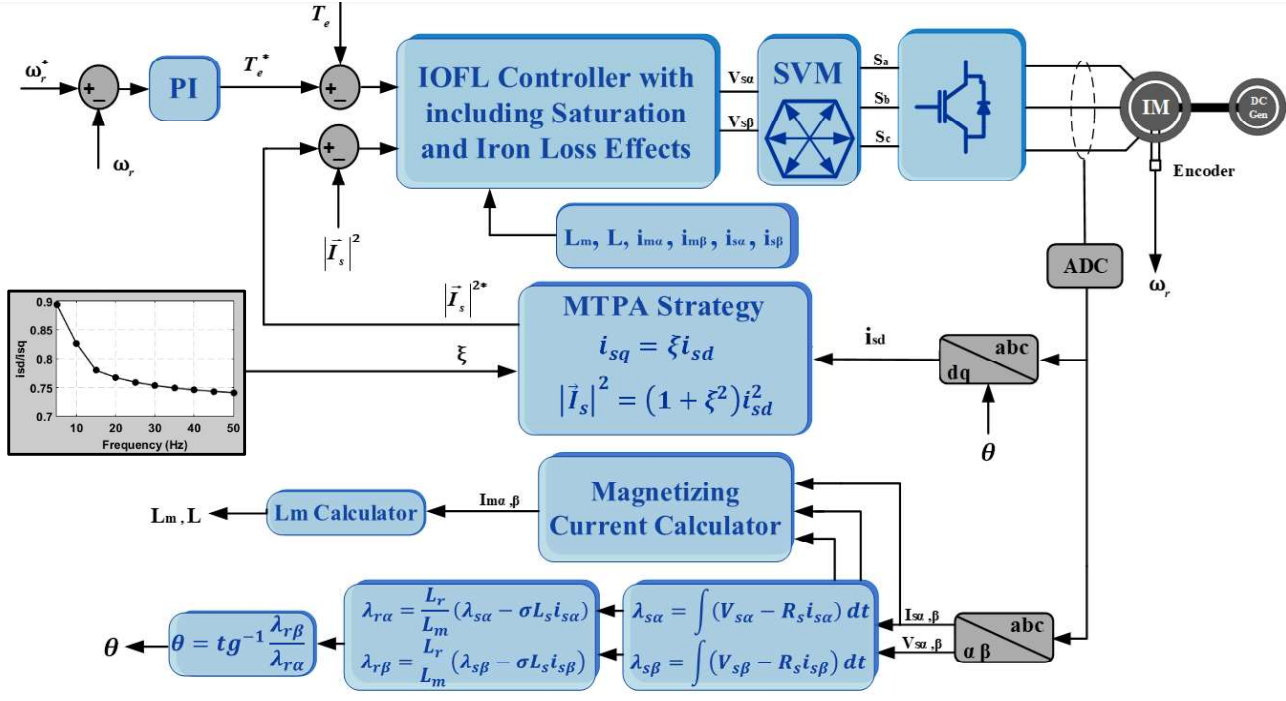


Fig. 10. The block diagram of the induction motor drive system.

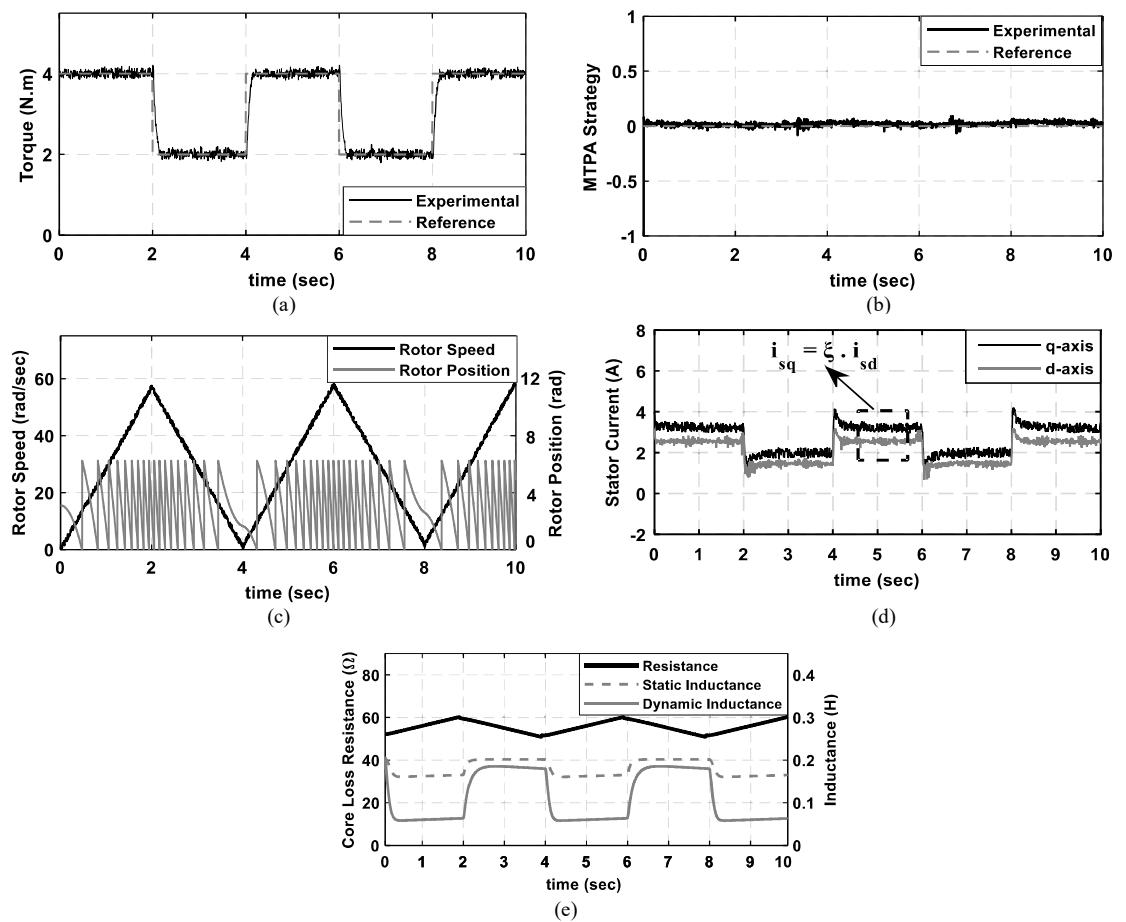


Fig. 11. Experimental results for torque control: (a) electromagnetic torque, (b) MTPA realization criterion, (c) rotor speed and position, (d) d- and q- axis components of the stator currents at the rotor flux reference frame, (e) variations of static and dynamic inductances and the core loss resistance.

When the rotor speed varies, the frequency and consequently the iron loss resistance varies accordingly. Fig. 11(e) shows that how this resistance varies with the rotor speed change. Variations of static and dynamic inductances versus time are also illustrated in Fig. 11(e). To investigate the effect of load torque perturbations on the performance of the controller, an additional experimental scenario is tested in the lab. In this test, the performance of the MTPA is validated when the closed-loop speed control is added to the control structure. Under this condition, the reference electromagnetic torque is obtained from the output of the speed controller and the rotor speed is controlled at $\omega_r = 80$ rad/sec (Fig. 12(a)). The electromagnetic torque is plotted in Fig. 12(c), when the load torque steps up from 2 N·m at the nominal flux to 4 N·m. To achieve the conventional field-oriented control, the MTPA control loop is replaced by a flux control loop, and the nominal motor flux is selected as the reference flux. As expected, the proposed MTPA strategy leads to a lower stator current magnitude than the constant flux method. Such reduction is more significant under light loads.

In Figs. 13(a) and 13(b), trajectories of the stator's two-axis flux are drawn for the two scenarios of previous test (with and without the MTPA strategy). The circle shapes indicate that the applied three phase voltages to the motor were balanced.

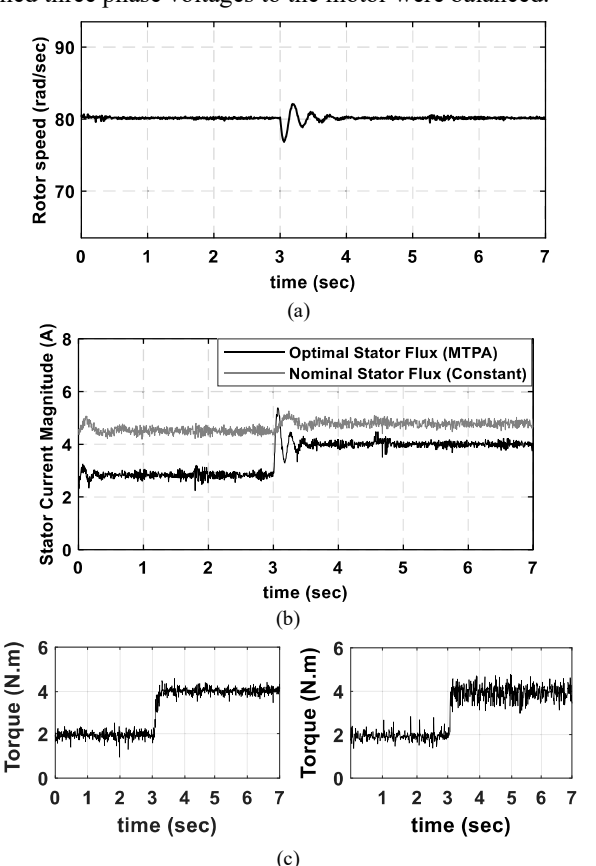


Fig. 12. Experimental results for speed control: (a) rotor speed, (b) stator current magnitude, (c) Electromagnetic torque (Reference torque: left side, Measured torque: Right side).

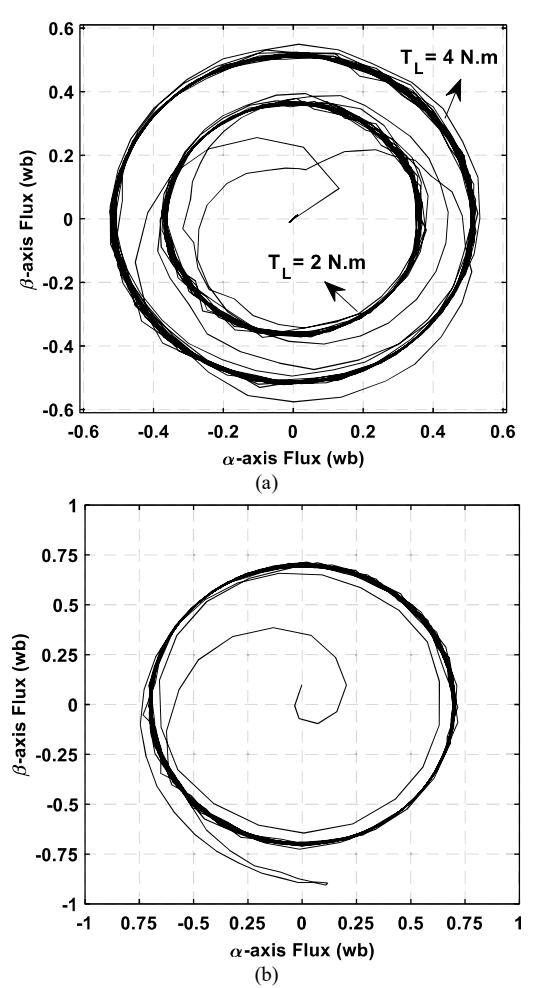


Fig. 13. Stator flux trajectory: (a) With MTPA strategy, (b) Without MTPA strategy.

In Fig. 13(a) with the MTPA strategy, the magnitude of stator flux varies with the load torque, which indicates that the MTPA strategy indirectly adjusts the stator flux to an optimal value to achieve the given electromagnetic torque and speed. According to Fig. 14, under non-ideal conditions, the stator current magnitude is approximately decreased by 10.8% compared to the ideal condition, for 25% of rated torque. In fact, the reduction of stator current magnitude is more significant under light load conditions.

To study the sensitivity of the proposed controller to the motor parameter variations, the relative changes in $|\vec{l}_s|$ due to R_s , R_r and J (the moment of inertia) are shown in Fig. 15 for $T_l = 4 \text{ N·m}$ and $\omega_r = 50 \text{ rad/sec}$. These plots indicate that the controller is more sensitive to errors in R_s and R_r than in J. If the moment of inertia has an accuracy of $\pm 50\%$, the variation of $|\vec{l}_s|$ is within $\pm 1\%$. However, R_s and R_r must have an accuracy of $\pm 25\%$ to maintain the variation of $|\vec{l}_s|$ within $\pm 1\%$.

VI. CONCLUSION

The IOFL-based highly efficient nonlinear controller is presented in this paper for dynamic direct torque control of IMs by considering saturation effect and iron losses. Unlike the

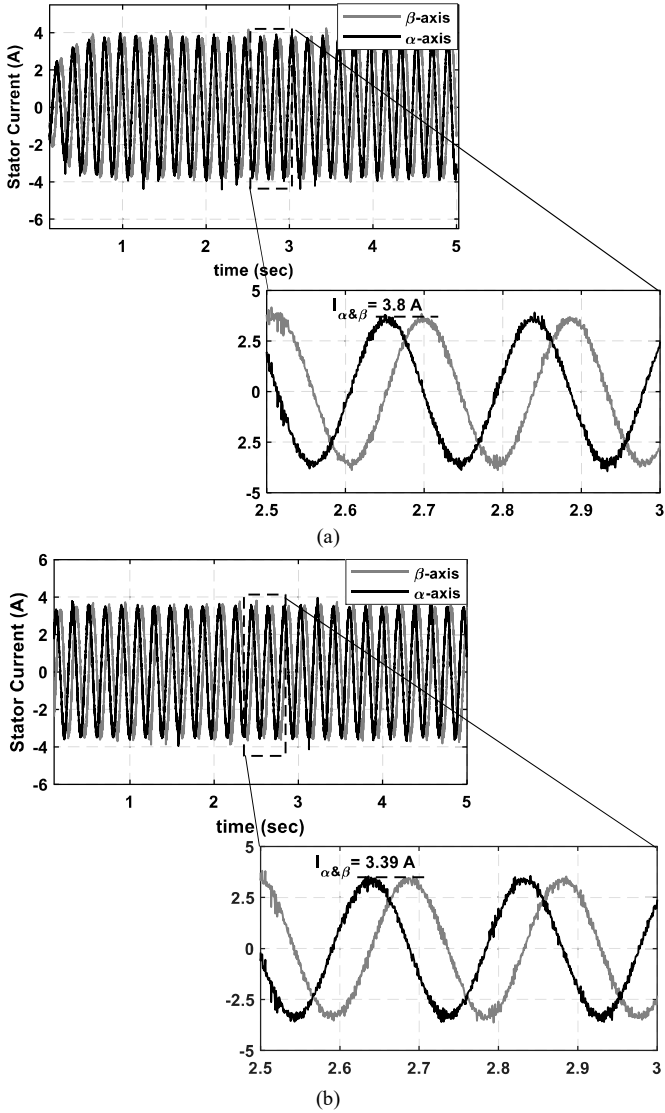


Fig. 14. Experimental result for D- and Q-axis components of the stator current at the stationary reference frame for 25% of rated torque (speed control): (a) without considering the iron loss resistance and magnetic saturation (Ideal condition), (b) with considering the iron loss resistance and magnetic saturation (Non ideal condition).

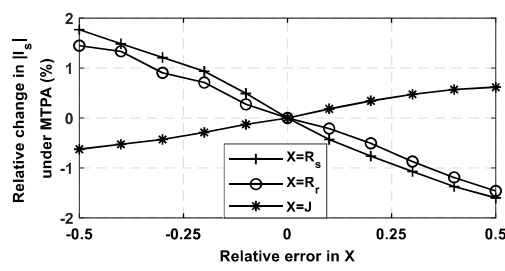


Fig. 15. Relative changes in the minimum value of the stator current magnitude vs. errors in R_s , R_r and J

conventional DTC, in which the direct axis control input is determined based on the nominal flux, the optimal flux is obtained using a novel MTPA strategy in the proposed control scheme. The electromagnetic torque and the MTPA criterion are both directly regulated by the developed controller. The proposed IOFL approach is developed using a novel formulation of the IM dynamic model by considering magnetic saturation and iron losses and it is expressed in a space-state form in the stationary reference frame. In order to do this, a special consideration was given to the selection of the nonlinear functions interpolating the magnetic parameters in terms of the magnetizing current. The cross-saturation term is considered to improve the model accuracy. Experiments were conducted in the lab to demonstrate the effectiveness of the suggested control method. Experimental results show that the stator current magnitude can be reduced compared to when the constant flux control method is used, by implementing the proposed MTPA strategy. In contrast to the ideal condition, in which the two-axis components of stator current are equal, the ratio of q-axis to d-axis stator current was shown to be dependent on the variations of the iron loss resistance and magnetizing inductance.

APPENDIX

To determine the magnetizing curve, the no load test was performed at the rated frequency and different voltages, started by applying a low voltage of 52.07 V, and gradually increased to 178.8 V, as shown in Table II. For each voltage level, the corresponding current and magnetic flux density were measured, and the magnetizing curve can then be determined by plotting the magnetic flux linkage versus the magnetizing current. The magnetizing flux based on the interpolating curve is proposed as an exponential function as follows:

$$\lambda_m = 0.54365 - 0.55214 \, e^{-0.381275 \, l_m^{1.84665}} \tag{43} \label{eq:lambda}$$

Also, static and dynamic inductances can be computed by (6) as follows:

$$L_m = (0.54365 - 0.55214 e^{-0.381275 I_m^{1.84665}} / I_m)$$
(44)

$$L_m = (0.54365 - 0.55214 e^{-0.381275 I_m^{1.84665}} / I_m)$$

$$L = 0.38875 I_m^{0.84665} e^{-0.381275 I_m^{1.84665}}$$
(45)

Fig. A-1 illustrates variations of L_m and L with the magnetizing current. The magnetizing current must be computed to determine the magnetizing inductance using the λ - i_m curve. Based on the two-axis stator flux and current values, the magnetizing current relationship can be determined

TABLE II NO LOAD TEST RESULTS

110 LOAD TEST RESULTS					
$V_{ph}\left(\mathbf{V}\right)$	$I_m(A)$	$X_m\left(\Omega\right)$	L_m (H)	λ_m (wb)	
52.07	1.08	48.21	0.1534	0.16573	
63.68	1.19	53.512	0.17	0.2023	
75.28	1.21	62.214	0.198	0.2395	
86.71	1.37	63.292	0.2014	0.276	
98.61	1.51	65.304	0.20786	0.3138	
110.27	1.67	66.029	0.21	0.3509	
122.39	1.84	66.516	0.2117	0.389	
133.94	2.19	61.159	0.194	0.426	
144.33	2.44	59.151	0.188	0.459	
155.88	3	51.96	0.1653	0.496	
167.43	3.69	45.373	0.1444	0.5329	
173.2	4.03	42.977	0.1368	0.5513	
176.14	4.5	39.144	0.1246	0.5595	
177.5	5	35.5	0.113	0.565	
178.8	5.635	31.73	0.101	0.57	

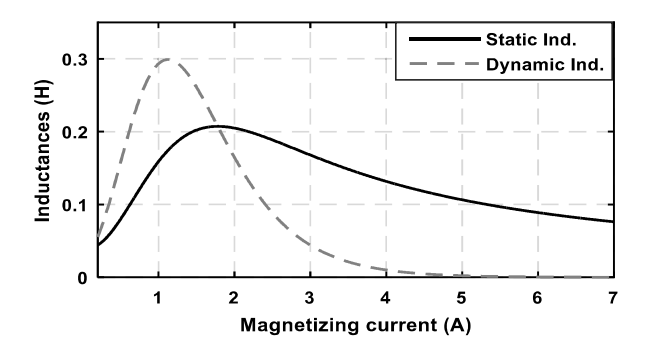


Fig. A-1. Static and dynamic inductances under no load condition at the rated frequency and different voltages.

$$i_{m\alpha} = \frac{\lambda_{s\alpha} - L_{ls}i_{s\alpha}}{L_m}$$

$$i_{m\beta} = \frac{\lambda_{s\beta} - L_{ls}i_{s\beta}}{L_m}$$
(46)

$$i_{m\beta} = \frac{\lambda_{s\beta} - L_{ls}i_{s\beta}}{L_{m}} \tag{47}$$

By substituting (44) into the denominator of the two-axis magnetizing current equation in the stationary reference frame and solving the resulting equation, both the magnetizing current and the variable magnetizing inductance under different loading conditions can be determined. At each computation step, the value of the magnetizing inductance obtained in the previous step is used to calculate new values of the magnetizing current components.

REFERENCES

- [1] T. Ayana, P. Kolodziejek, M. Morawiec and L. Wogi "Loss Minimization Based Sensorless Control of High-Speed Induction Motor Considering Core Loss," IEEE Access, Aug. 2024.
- S. Cosso, K. Kumar, M. Marchesoni, M. Passalacqua and L. Vaccaro, "Stability Issues in V/f Controlled Medium Voltage Induction Motor Drives Considering Magnetizing Inductance Variation," in IEEE Transactions on Energy Conversion, vol. 38, no. 4, pp. 2909-2918, Dec.
- M. N. Uddin, and S. W. Nam, "Development and Implementation of a Nonlinear-Controller-Based IM Drive Incorporating Iron Loss with Parameter Uncertainties," IEEE Trans. Ind. Electron., vol. 56, no. 4, pp. 1263-1272, 2009.
- E. Levi, S. Vukosavic, and V. Vuckovic, "Saturation Compensation Schemes for Vector Controlled Induction Motor Drives " Conf. Rec. IEEE Power Elect. Specialists Conf., pp. 591-598, 1990.
- L. Liu, X. Du, and S. Shen, "Indirect Field-Oriented Torque Control of Induction Motor Considering Magnetic Saturation Effect: Error Analysis," IET Electr. Power Appl., vol. 11, no. 6, pp. 1105–1113, 2017.
- D. Dolinar, P. Ljušev, and G. Štumberger, "Input-output linearizing tracking control of an induction motor including magnetic saturation effects," IEE Proceedings-Electric Power Applications, vol. 150, no. 6, pp. 703-711, Nov. 2003.
- M. Sokola and E. Levi, "Combined impact of iron loss and main flux saturation on operation of vector-controlled induction machines," Sixth International Conference on Power Electronics and Variable Speed Drives, Conf. Publ. No. 429, Nottingham, UK. 1996.
- Y. Zeng, M. Cheng, X. Wei, and L. Xu, "Dynamic Modeling and Performance Analysis with Iron Saturation for Dual-Stator Brushless Doubly Fed Induction Generator," IEEE Trans. Energy Convers, vol. 35, no. 1, pp. 260-270, Mar. 2020.
- A. Borisevich, G. Schullerus, "Energy efficient control of an induction machine under torque step changes", IEEE Trans. Energy Convers., vol. 14, no. 8, pp. 1295-1303, Dec. 2016.
- O. Kiselychnyk, M. Bodson, and J. Wang, "Comparison of Two Magnetic Saturation Models of Induction Machines and Experimental Validation.' IEEE Trans. Ind. Electron., vol. 64, no. 1, pp. 81–90, Jan. 2017.
- [11] H. Mosaddegh Hesar, M. A. Salahmanesh and H. Abootorabi Zarchi, "Generalized Analysis of Brushless Doubly Fed Induction Machine

- Taking Magnetic Saturation and Iron Loss into Account," IEEE Transactions on Industrial Electronics, vol. 68, no. 8, pp. 6470-6480, Aug. 2021.
- [12] P. Vas, "Generalized Analysis of Saturated AC Machines," vol. 64, pp. 57-62, 1981.
- [13] M. Pucci, "State-space space-vector model of the induction motor including magnetic saturation and iron losses," IEEE Trans. Ind Appl., vol. 55, no. 4, pp. 3453-3468, Jul./Aug. 2019.
- [14] E. Levi, "A unified approach to main flux saturation modelling in D-O axis models of induction machines," IEEE Trans. Energy Conv., vol. 10, no. 3, pp. 455-461, Sep. 1995.
- [15] E. Levi, "Impact of cross-saturation on accuracy of saturated induction machine models", IEEE Trans. Energy Convers., vol. 12, no. 3, pp. 211-216. Sep. 1997.
- [16] I. Boldea and S. A. Nasar, "Unified treatment of core losses and saturation in the orthogonal-axis model of electric machines," Proc. Inst. Elect. Eng., pt. B, vol. 134, no. 6, pp. 355-363, Nov. 1987.
- [17] M. A. Salahmanesh, H. Abootorabi Zarchi, and H. Mosaddegh-Hesar, 'Lyapunov -Based Input-Output Feedback Linearisation Control of Induction Motor drives Considering Online MTPA Strategy and Iron Loss," ICEE 2019 - 27th Iran. Conf. Electr. Eng., pp. 697-701, 2019.
- [18] J. E. Slotine, and W. Li, "Applied Nonlinear Control", Prentice-Hall, Englewood Cliffs, 1991.
- [19] A. Accetta, F. Alonge, M. Cirrincione, M. Pucci, and A. Sferlazza, Feedback Linearizing Control of Induction Motor Considering Magnetic Saturation Effects," IEEE Trans. Ind. Appl., vol. 52, no. 6, pp. 4843-4854, Nov./Dec. 2016.
- [20] M. N. Uddin, S. W. Nam, "New online loss-minimization-based control of an induction motor drive", IEEE Trans. Power Electron., vol. 23, no. 2, pp. 926-933, Mar. 2008.
- [21] M. Hajian, J. Soltani, G. A. Markadeh, and S. Hosseinnia, "Adaptive Nonlinear Direct Torque Control of Sensorless IM Drives with Efficiency Optimization," IEEE Trans. Ind. Electron., vol. 57, no. 3, pp. 975-985, Mar. 2010.
- [22] S. Bolognani, L. Peretti and M. Zigliotto, "Online MTPA Control Strategy for DTC Synchronous-Reluctance-Motor Drives," IEEE Transactions on Power Electronics, vol. 26, no. 1, pp. 20-28, Jan. 2011.
- [23] R. R. Chowdhury, G. Koperundevi and A. Venkadesan, "Simplified MTPA Integrated Virtual Voltage Vector-Based MPCC for Improved Performance and Efficiency in IM Drive-Based Electric Vehicles," in IEEE Transactions on Transportation Electrification, vol. 11, no. 2, pp. 6753-6762, April 2025.
- [24] C. Jain, N. Vaishnav and A. K. Jain, "MTPA Control of Double Inverter Fed Wound Rotor Induction Motor Drive," in IEEE Transactions on Energy Conversion, vol. 38, no. 4, pp. 2326-2343, Dec. 2023.
- A. Fereidooni, S. A. Davari, C. Garcia and J. Rodriguez, "Simplified Predictive Stator Current Phase Angle Control of Induction Motor with a Reference Manipulation Technique," IEEE Access, vol. 9, pp. 54173-54183, 2021.
- [26] K. Lee and Y. Han, "Reactive-Power-Based Robust MTPA Control for v/f Scalar-Controlled Induction Motor Drives," IEEE Transactions on Industrial Electronics, vol. 69, no. 1, pp. 169-178, Jan. 2022.
- P. Naganathan and S. Srinivas, "MTPA Associated DTC Methodologies for Enhanced Performance and Energy Savings in Electric Vehicle Mobility with Induction Motor Drive," IEEE Transactions on Transportation Electrification, vol. 8, no. 2, pp. 1853-1862, June 2022.
- T. Windisch and W. Hofmann, "A Novel Approach to MTPA Tracking Control of AC Drives in Vehicle Propulsion Systems," IEEE Transactions on Vehicular Technology, vol. 67, no. 10, pp. 9294-9302, Oct. 2018.
- [29] S. Bozhko, S. Dymko, S. Kovbasa and S. M. Peresada, "Maximum Torque-per-Amp Control for Traction IM Drives: Theory and Experimental Results," IEEE Transactions on Industry Applications, vol. 53, no. 1, pp. 181-193, Jan.-Feb. 2017.
- [30] O. Wasynczuk, S. D. Sudhoff, K. A. Corzine, J. L. Tichenor, P. C. Krause, I. G. Hansen and L. M. Taylor, "A Maximum Torque per Ampere Control Strategy for Induction Motor Drives", IEEE Transactions on Energy Conversion, vol. 13, no. 2, pp. 163-169, June 1998.
- [31] R. Bojoi, Z. Li, S. A. Odhano, G. Griva and A. Tenconi, "Unified Direct-Flux Vector Control of Induction Motor Drives with Maximum Torque per Ampere Operation", Energy Conversion Congress and Exposition (ECCE), September 2013.
- [32] A. Ahmed, B. Kwon Koh, J. Kim and Y. Lee, "Finite Control Set-Model Predictive Speed Control for Induction Motors with Optimal Duration", 20th IFAC World Congress, vol. 50, no. 1, pp. 7801-7806, July 2017.

- [33] Test Procedure for Poly-phase Induction Motors and Generators, IEEE Standard 112 (Revision of IEEE Std 112-2004), 2017.
- [34] E. Levi, M. Sokola, A. Boglietti and M. Pastorelli, "Iron Loss in Rotor-Flux-Oriented Induction Machines: Identification, Assessment of Detuning, and Compensation," *IEEE Transactions on Power Electronics*, vol. 11, no. 5, pp. 698-709, Sept. 1996.
- [35] K. Matsuse, T. Yoshizumi, S. Katsuta and S. Taniguchi, "High-Response Flux Control of Direct-Field-Oriented Induction Motor with High Efficiency Taking Core Loss into Account," *IEEE Transactions on Industry Applications*, vol. 35, no. 1, pp. 62-69, Jan.-Feb. 1999.
 [36] V. Popovic, D. Oros and D. Marcetic, "MAPT Strategy of IM Including
- [36] V. Popovic, D. Oros and D. Marcetic, "MAPT Strategy of IM Including Iron Loss Phenomena," International Symposium on Industrial Electronics and Applications (INDEL), Banja Luka, Bosnia and Herzegovina, 2020.



Mohammad Ali Salahmanesh received the M.Sc. (With hons.) degree in electrical engineering in 2019 from Ferdowsi University of Mashhad, Mashhad, Iran, where he is currently working toward the Ph.D. degree in electrical machines and drives. His research interests include control of electrical drives, design and modeling of electrical machines.



Hossein Abootorabi Zarchi received his M.S. and Ph.D. degrees in Electrical Engineering from Isfahan University of Technology, Isfahan, Iran, in 2004 and 2010, respectively. He served as a Visiting Professor in the Department of Electrical and Computer Engineering at the University of Saskatchewan, Saskatoon, SK, Canada, from July 2024 to June 2025. He is currently an Associate Professor in the Department of Electrical Engineering at Ferdowsi University of Mashhad, Mashhad, Iran, and also

serves as an Associate Researcher in the Department of Electrical and Computer Engineering at Queen's University, Ontario, Canada. His research interests include electrical machines and drives, applied nonlinear control, and renewable energy systems.



Salman Abdi (Senior Member, IEEE) received the B.Sc. degree in electrical engineering from the Ferdowsi University, Mashhad, Iran, in 2009, the M.Sc. degree in electrical engineering from the Sharid University of Technology, Tehran, Iran, in 2011, and the Ph.D. degree in electrical machines design and optimization from the Cambridge University, Cambridge, U.K, in 2015. He is currently an Associate

Professor in electrical engineering with the University of East Anglia, Norwich, U.K. His research interests include electrical machine design, modeling, optimisation and fault diagnosis for renewable power generation and electric propulsion systems.



Hamidreza Mosaddegh-Hesar received his Ph.D. degree in Electrical Engineering from Ferdowsi University of Mashhad, Iran, in 2019. He is currently a Senior Researcher with Huawei Technologies, Canada. His research interests include electrical machines and drives, power electronics, and renewable energy systems.



Xiaodong Liang (M'06–SM'09) was born in Lingyuan, Liaoning, China. She received the B.Eng. and M.Eng. degrees from Shenyang Polytechnic University, Shenyang, China in 1992 and 1995, respectively, the M.Sc. degree from the University of Saskatchewan, Saskatoon, Canada in 2004, and the Ph.D. degree from the University of Alberta, Edmonton, Canada in 2013, all in electrical engineering.

From 1995 to 1999, she served as a lecturer at Northeastern University, Shenyang, China. In October 2001, she joined Schlumberger (SLB) in Edmonton,

Canada, and was promoted to a Principal Power Systems Engineer with this world's leading oilfield services company in 2009; she worked with Schlumberger for almost 12 years until August 2013. From 2013 to 2019, she was with Washington State University in Vancouver, WA, United States and Memorial University of Newfoundland in St. John's, NL, Canada as an Assistant Professor and later an Associate Professor. In July 2019, she joined the University of Saskatchewan in Saskatoon, Canada, where she is currently a full Professor and Canada Research Chair in Technology Solutions for Energy Security in Remote, Northern, and Indigenous Communities. She was an Adjunct Professor with Memorial University of Newfoundland from 2019 to 2022. Her research interests include power systems, renewable energy, and electric machines.

Dr. Liang is the registered Professional Engineer in the province of Saskatchewan, Canada, the Fellow of IET, and the Deputy Editor-in-Chief of IEEE Transactions on Industry Applications, the Co-Editor-in-Chief of IEEE Canadian Journal of Electrical and Computer Engineering, and Member-at-Large at IEEE Industry Applications Society.